# DESIGN OF SELF-REGULATED FLOW CONTROL MECHANISM FOR A TURBOCHARGER GAS STAND TEST FACILITY

**Article history**
Received
*8th September 2021*
Revised
*12th June 2022*
Accepted
*12th June 2022*
Published
*22nd June 2022*

Chun Mein Soon[1], Meng Soon Chiong[1,2*], Mahadhir Mohammad[1], Muhammad Hanafi Md Shah[1], Muthuramalinga Tevar[2]

[1] UTM LoCARtic, IVeSE,
Universiti Teknologi Malaysia, 81310 UTM Johor Bahru, Johor, Malaysia

[2] School of Mechanical Engineering, Faculty of Engineering
Universiti Teknologi Malaysia, 81310 UTM Johor Bahru, Johor, Malaysia

[*]Corresponding email: chiongms@utm.my

## ABSTRACT

*A turbocharger test facility is essential to evaluate the turbocharger's performance by mapping the turbine and compressor operating conditions. This paper aims to design a self-regulated airflow control mechanism for the turbocharger test facility in UTM LoCARtic. Previously, the gas stand airflow was regulated manually. However, the vast variety of turbocharger design and operating conditions increase the difficulty to continuously and precisely regulate the airflow manually. In this paper, the valve and actuator selection, the mechanical design and the control loop design will be presented. Four valves model have been considered, namely globe type, ball type, butterfly valve and gate valve. The final selection was based on the flow coefficient ($K_v$), pressure drop, stability and accuracy. The actuation system is also one major consideration to obtain the best accuracy and response time. An electric actuator helps to achieve a self-regulated flow control mechanism. In conclusion, the globe type valve was chosen because of the flow accuracy, flow stability and the $K_v$ value is close to the gas stand's requirement.*

**Keywords**: *Turbocharger gas stand, Flow Control Mechanism, Control Valve, Self-regulated.*



## 1.0 INTRODUCTION

Nowadays, a turbocharger is widely used on modern internal combustion engines to improve the efficiency of the engine by circulating the exhaust air to run the turbine and compressor [1]. A turbocharger increases the air density entering the intake manifold to boost the power of engine output. The engine performance is highly dependent on how well a turbocharger is matched to the engine. The engine-turbocharger matching is done based on the turbocharger's performance characteristic map. A turbocharger gas stand is needed to measure the turbocharger performance. Figure 1 shows the schematic view of a typical turbocharger gas stand [2]. In the gas stand, the flow control mechanism is one of the most important systems. It regulates the pressure ratio of the turbine and compressor to achieve the desired turbocharger conditions.

 DOI: https://doi.org/10.11113/jm.v45.453

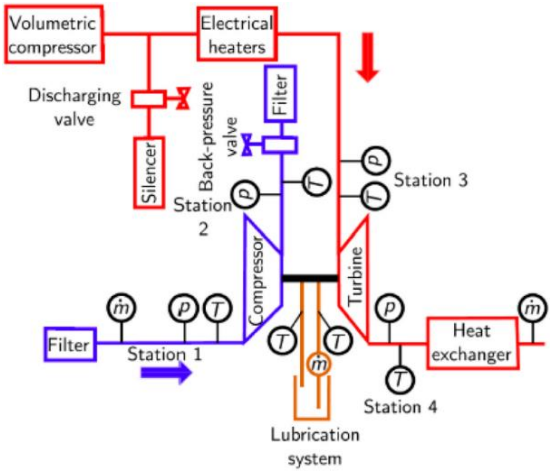


**Figure 1**: Schematic view of a typical turbocharger gas stand [2]

The turbine inlet temperature, turbine inlet mass flow rate, compression ratio and turbocharger speed can be manipulated on the gas stand test to achieve different turbocharger operating conditions [3]. To obtain a compressor or a turbine map it is necessary to know the following variables at each operating point such as mass flow rate, pressure ratio and turbocharger speed. Turbocharger performance mapping is done by first choosing the initial turbocharger speed by varying the turbine inlet pressure. The compressor pressure ratio is then fixed by regulating the compressor outlet pressure. In the process, the turbine inlet pressure may need to be compensated to maintain a constant turbocharger speed. The resultant pressure, pressure drop, and temperature readings are taken to calculate the turbocharger mass flow rate. The process is repeated for different compressor pressure ratios and then different turbocharger speeds to become the turbocharger performance map.

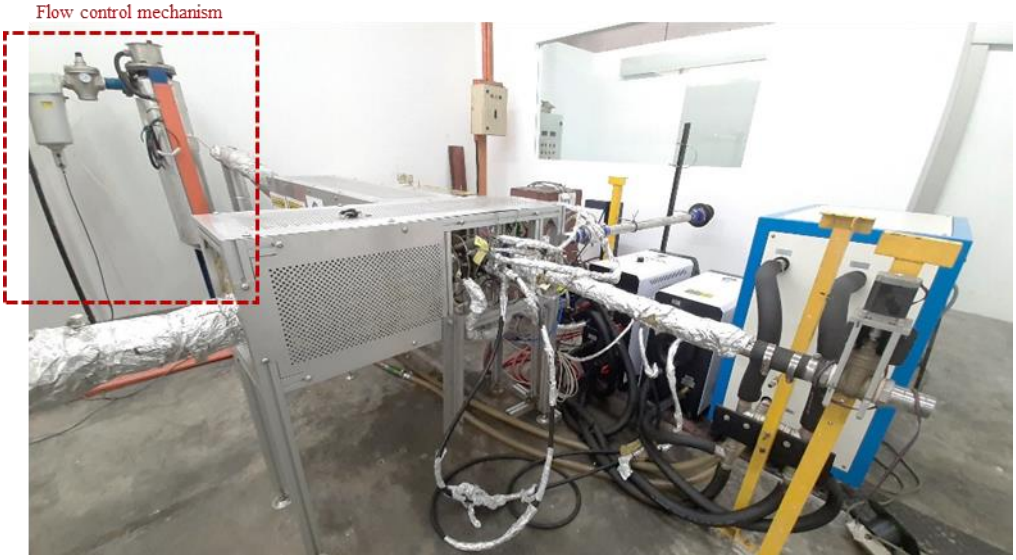


**Figure 2**: UTM LoCARtic turbocharger gas stand test facility setup

This paper aims to design a self-regulated flow control mechanism for the UTM LoCARtic turbocharger test facility. Figure 2 shows the layout of the gas stand and Figure 3 shows the existing manual flow control mechanism. The compressed air flow entering the turbine inlet was controlled only via a manual pressure regulator. Consequently, the pressure regulator needs to be constantly adjusted manually throughout the test for different operating conditions. Not only it was less accurate, but manual operation during turbocharger testing also posed a serious safety hazard to the operators. Furthermore during

 DOI: https://doi.org/10.11113/jm.v45.453

the turbocharger surging, the controlling the turbocharger mass flow even harder due to flow instability. Hence with the help of the new control valve and new closed loop control will improve the test flow stability. Therefore scope of this paper cover the following,

i. Control valve selection
ii. Control valve design
iii. Control valve control system

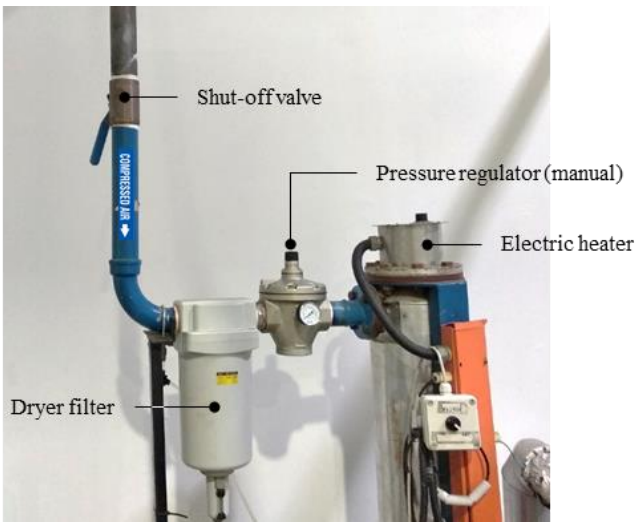


**Figure 3**: Existing gas stand flow control mechanism

## 2.0 LITERATURE REVIEW

This section provides a review of the control valves application, type of control valve and actuators readily available on the market. The advantages and disadvantages of each type of control valve and actuator will be discussed.

Control valves are commonly used in industry to regulate or throttle the flow rate. In advance application, control use to increase the system performances. Use of control valve in supercritical $CO_2$ Brayton Cycle provide a better load regulation. When the valve opening reduced to 50%, a load rate 40.87% and 52.33% can be achieved. Furthermore, its provide real time tracking and act as safety system shut off valve [4]. Furthermore, right number of valve and correct scheduling operating time at steam turbine power plant increase the efficiency as much as 531616 kWh and higher water quality entering steam turbine [5]. Valves are not just use to regulate conventional fluid such as water, gas and oil, but in advance application use to regulate the high pressure hydrogen [6].

In proper valve selection can cause damaged to valve or operational error. In example, ball valve not suitable for continuous throttling in harsh environment, but the glove valve are highly recommended to control the flow rate [7]. Ball valve suitable for on and off the flow stream. Alternative for ball valve is butterfly valve good for start and stop application. Y-pattern globe valves proposed for fluid controlling instead of straight pattern glove valve to minimize the risk of wear and internal cavitation [8].

Control valve also used in turbocharger test rig. Control valve used to regulate compressor mass flow at constant turbocharger speed [9]. Furthermore, use of control valve helps the control strategies in two stage turbocharger mapping procedure [10]. Ball valve also being use to regulate the pressure ratio and mass flow on turbocharger test rig [11]. Having a pressure regulator before control valve also helps the flow stability during the experiment especially during unsteady performances evaluation [12]. Therefore, getting a

 DOI: https://doi.org/10.11113/jm.v45.453

best control valve for turbocharger test rig is very important to ensure the result from the experiment is accurate and small uncertainty.

## 2.1 Types of Control Valves

Valves are commonly available with many varieties of design, connection, material and size. The selection of valve is mainly dependent on the working condition, load characteristics and task. For example, the highest's strain values were observed at a globe valve's transition area, sphere to cylinder junction which the valve body material is affected by the developed pressure in the fluid stream [13]. The most common types of valves are butterfly valve, ball valve, gate valve and globe valve [14] as shown in Figure 4. The details for each of these control valves are compared in Table 1.

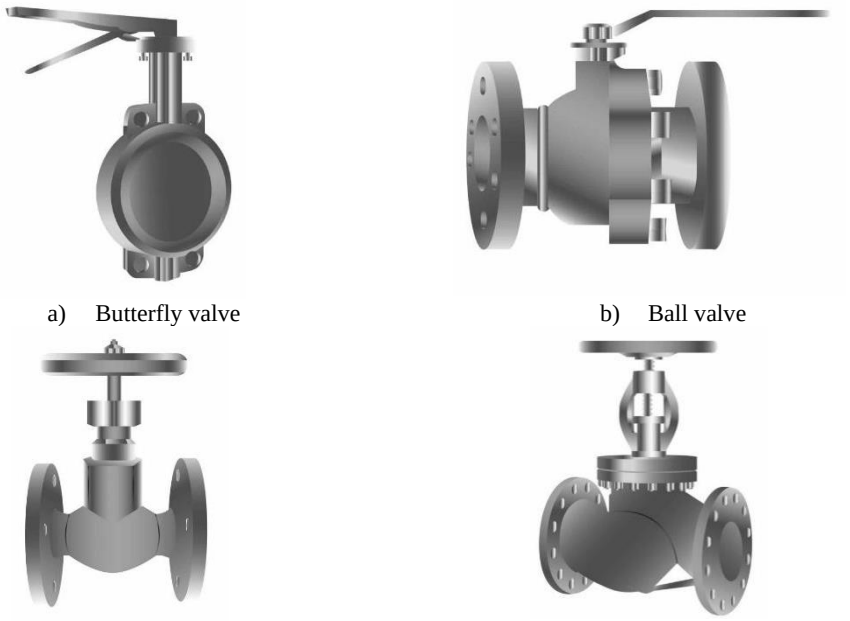

a) Butterfly valve b) Ball valve

c) Gate valve d) Globe valve

**Figure 4**: Common types of control valve [5]

**Table 1**: Advantages, Disadvantages and $K_v$ for different types of valve [14], [15]

| Valve type | Advantages | Disadvantages | Flow Coefficient, $K_v$ |
|---|---|---|---|
| Butterfly valve | Low maintenance, high flow capacity. | Require high torque to control and prone to cavitation at lower flows. | 61 |
| Ball valve | High flow capacity and withstand high pressure and temperature. | Less throttling property and prone to cavitation. | 134 |
| Gate valve | Tight shut-off and ability to cut through slurries. | Low pressure limitation and not suitable for throttling. | 112 |
| Globe valve | Efficient and precise throttling and accurate flow control. | Higher pressure drop and low coefficient of flow. | 19 |


DOI: https://doi.org/10.11113/jm.v45.453

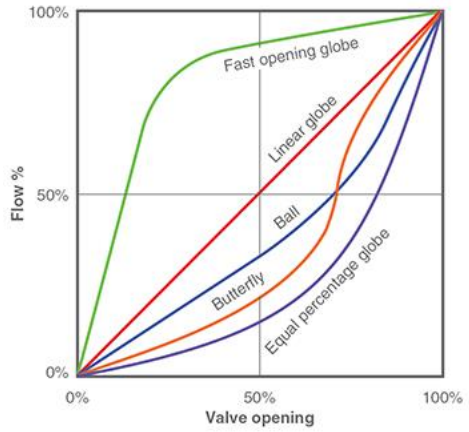


**Figure 5**: Inherent flow characteristics of some typical valves [7]

Figure 5 shows the inherent flow characteristics of these valve types. The flow characteristic of a globe valve is defined as the relationship between valve stem travel and control valve capacity. The trim design of a globe valve will affect the changes of flow capacity through the valve as the plug travels completely [16]. Flow coefficient, $K_v$, defines the flow rate in cubic meters per hour ($m^3/h$) of water at a temperature of 16 °C with a pressure drop of 1.0 bar across the valve [17]. $K_v$ value plays important role in valve selection as it will be used to calculate the flow capacity of the valve at a given pressure difference and temperature.

## 2.2 Type of Valve Actuators

A valve actuator is a device that actuates the valve to different openings. The actuator could be powered manually (through lever and gear), electrically or pneumatically (via pressure difference and diaphragm). A basic actuator turns the valve either fully close or fully open, while a modern actuator can control the valve opening with a higher degree of accuracy [14]. This can also be done remotely. There are two common types of actuators widely available, namely the pneumatic and electric actuators, as shown in Figure 6. There are other types of actuators available in the market, but these two are the most popular choice in industries today in terms of controllability and working conditions.

Both actuators have their pros and cons depending on their work environment. Table 2 shows the advantage and disadvantage comparison between pneumatic and electric actuators. An electric actuator is responding faster, more precisely and accurately but comes with a pricy cost trade-off. Actuator sizing is based on the required thrust force to overcome the flow-induced force acting on the globe valve. The flow-induced force consists of two components: axial and transverse force. The largest axial force occurs at the minimum or close position. As the valve opening becomes larger, the axial force reduces [18].

a) Pneumatic actuator b) Electric actuator

**Figure 6**: Types of valve actuator

 DOI: https://doi.org/10.11113/jm.v45.453

**Table 2**: Advantages and disadvantages of different actuator types [19]

| Actuator type | Advantages | Disadvantages | Accuracy | Repeatability |
|---|---|---|---|---|
| Pneumatic actuator | Provide high speed and force. | Delayed response and high maintenance cost. | 0.1 inches | 0.001 inches |
| Electric actuator | Provide precise control and positioning, quick response and high degree of stability. | Expensive and can only be used in a safe, rendered environment. | 0.000315 inches | 0.0000394 inches |

## 3.0 METHODOLOGY

An electrical valve actuator is selected to replace the existing manual control valve on the UTM LoCARtic turbocharger gas stand. For this new setup, a control system is needed to control the actuator at various operating condition. In this context, a closed-loop Proportional-Integral-Derivative (PID) controller is designed and implemented using NI LABVIEW software. The objective of the control system is to maintain a target turbocharger speed at different inlet pressure (air flow rate) and compressor pressure ratio (loading) by actuating the electrical valve.

On the other hand, various types of control valves, materials, standards and flow coefficients were considered to select the most suitable control valve. After the selection process, the chosen valve is modelled in CAD software along with its actuator and auxiliary system.

### 3.1 Available Control Valve and Actuators

Two valve models have been shortlisted for the final selection. First model is Spirax Sacro (Spira-Trol) and second model is Armaturen (Ari-Steri). The control valve selection is based on the compressed air flow conditions shown in Table 3. Both final models are globe type since it well-known for accurate flow control as discussed in Section 2.1. Table 4 compares the specifications of these two control valves and Table 5 shows the comparison of their respective electric actuator.

**Table 3**: Control valve working conditions

| Parameters | Specifications |
|---|---|
| Type of fluid | Compressed dry air |
| Maximum inlet pressure, $P_1$ | 4.0 bar |
| Maximum outlet pressure, $P_2$ | 3.92 bar |
| Fluid temperature, $T$ | 60ºC |
| Maximum mass flow rate, $\dot{m}$ | 0.1 kg/s |
| Bore size | DN50 (2 inches) |

**Table 4**: Comparison of control valves

| Specification | Spirax Sarco | Armaturen |
|---|---|---|
| Valve model | Spira-tool | Ari-Stevi |
| Standard | ASME 125 | ASME 150 |
| Size | DN 50 | DN 50 |
| Material | Cast iron (ASTM A12B) | Ductile Iron (ASTM 395) |
| Plug | Parabolic | Parabolic |
| Steam seal | PTFE Chevron Seal | Spring Loaded PTFE V-ring |
| Rangeability | 30:1 | 50:1 |
| Joint | Flanged | Flanged |
| Seat | Metal to metal | Metal to metal |
| Flow factor, $K_v$ | 36.00 | 25.00 |
| Weight (kg) | 17.20 | 17.00 |
| Bonnet | Standard | Standard |
| Flange to flange length (mm) | 254 | 230 |


DOI: https://doi.org/10.11113/jm.v45.453

**Table 5**: Comparison of electric actuators

| Specification | Spirax Sarco | Armaturen |
|---|---|---|
| Actuator model | AEL 5 | Ari-Premio |
| Thrust (kN) | 1.00 | 2.20 |
| Speed of actuation (mm/s) | 0.25 | 0.38 |
| Weight (kg) | 4.50 | 5.40 |
| Stem travel (mm) | 50.00 | 50.00 |
| Voltage supply (V) | 230.00 | 230.00 |
| Power consumption (VA) | 25.50 | 21.00 |
| Maximum pressure difference (bar) | 5.60 | 20.00 |
| Feedback signal (mA) | 0.40 to 10.00 | 0.40 to 10.00 |

A motorized electric actuator is the most suitable actuator for the control system since it can be easily controlled via a computer program remotely. A linear electric actuator is the most appropriate electric actuator for the globe valve actuation. The linear electric actuators from the corresponding globe valves shown in Table 5 are largely similar in performance. The chosen globe valve and electric actuator will be integrated into the existing turbocharger test facility setup. The design of the new setup will be done in CAD software and presented in Section 4.4.

### 3.2 Flow Coefficient, $K_v$

The flow factor, also known as the flow coefficient, is the most important parameter in choosing a control valve [20]. The $K_v$ value represents the amount of flow that can get through the control valve at a specific condition. $K_v$ is generally a function of valve geometry and Reynolds number. Flow coefficient is in a linear relationship with the Reynolds number [21]. For small variation in flow Reynolds number, $K_v$ can be assumed constant while calculating the flow rate in valves for simplicity [22]. For the given condition in Table 3, the target $K_v$ for appropriate valve selection can be calculated using Equations 1 and 2 [23].

$$If\ \ P_2 < \frac{P_1}{2}, \qquad K_V = \frac{Q_N}{257\,.P_1}\sqrt{SG.T} \tag{1}$$

$$else\ if\ \ P_2 \geq \frac{P_1}{2}, \qquad K_V = \frac{Q_N}{514}\sqrt{\frac{SG.T}{\Delta P.P_2}} \tag{2}$$

The maximum mass flow rate, $\dot{m}$ = 0.1 kg/s and density of air at normal condition, $\rho_N$ defined by IUPAC at 0 ºC and atmospheric pressure condition is 1.2754 kg/m$^3$. The "normal" volume flow rate is calculated using equation 3 [23]:

$$Q_N = \frac{\dot{m}}{\rho_N} \tag{3}$$

Hence the $Q_N$ is 0.0784 m$^3$/s. From the condition given in Table 3 and the conditional Equations 1 and 2, the resultant $K_v$ = 17.9. This is the minimum required $K_v$ value for the selected globe valve.

### 3.3 Flow Rate Analysis on Control Valve

The objective of this analysis is to understand the relationship between the air mass flow rate and pressure drop across the valve. This analysis is done by varying the pressure drop at four different upstream pressure conditions. The operating conditions remained as in Table 3. The Ari-Stevi globe valve is chosen for this analysis as its $K_v$ value is closer to the design criteria. Since the $K_v$ valve is now known, Equations 1 and 2 are rearranged into Equations 4 and 5 to calculate the corresponding $Q_N$. From Table 4, the $K_v$ for Ari-Stevi

 DOI: https://doi.org/10.11113/jm.v45.453

globe valve is 25; and the allowable $Q_N$ = 394.25 m$^3$/h (0.1095 kg/s). This is sufficient for the operating condition in Table 3.

To calculate the mass flow rate, the air density at the outlet condition must be known. Therefore, the ideal gas relationship in Equation 6 is used to calculate the density of air at the outlet. The mass flow rate, $\dot{m}$ can then be calculated based on Equation 7. Hence, the Ari-Stevi globe valve can allow 0.4489 kg/s of mass flow rate at 4.0 bar upstream pressure and temperature of 60 °C. The resultant pressure drop across the globe valve is 0.08 bar. Thus, the selected valve is having a higher capacity than the maximum capacity of the turbocharger gas stand, which is 0.1 kg/s.

$$When\ \ P_2 < \frac{P_1}{2}, \qquad Q_N = \frac{257.K_V.P_1}{\sqrt{SG.T}} \tag{4}$$

$$When\ \ P_2 \geq \frac{P_1}{2}, \qquad Q_N = \frac{514.K_V}{\sqrt{\frac{SG.T}{\Delta P.P_2}}} \tag{5}$$

$$\rho = \frac{P_2}{RT} \tag{6}$$

$$\dot{m} = Q_N.\rho \tag{7}$$

### 3.4 Proposed Control Valve for the Flow Control Mechanism

After analyzing the valve characteristic based on the design requirement, the Ari-Stevi globe valve model is chosen for the turbocharger test rig. Furthermore, the Ari-Stevi globe valve comes with a matching electric actuator while for the Spira-tool globe valve, the actuator needs to be purchased separately. The minimum $K_v$ value has been calculated in Section 3.2, which is 17.9. The selected valve needs to have a higher $K_v$ than this minimum requirement because it can affect the pressure drop across the valve. However, the $K_v$ value should not be too large either or else the controllability may be compromised. The $K_v$ value of the Spira-tool globe valve (36.00) is much larger compared to the Ari-Stevi globe valve (25.00). The latter is preferable for the current application.

Furthermore, the rangeability of the Ari-Stevi globe valve is larger than the Spira-tool. Since turbocharger testing demands high accuracy, a larger rangeability valve can help to get an accurate result. The weight of the Ari-Stevi globe valve is also 0.2 kg lower than the Spira-tool. Once the valve selection is finalized, the corresponding linear electric actuator of the same brand is next selected. The comparison between the AEL5 actuator from Spirac Sarco and Ari-Premio actuator from Armaturen is made in Table 5.

Overall, their specifications are almost the same in terms of stem travel and power consumption. Yet the Ari-Premio actuator can actuate faster and with a higher thrust force. Figure 7 shows the selected Ari-Stevi globe valve with the Ari-Premio electric actuator and its corresponding CAD model.

 DOI: https://doi.org/10.11113/jm.v45.453

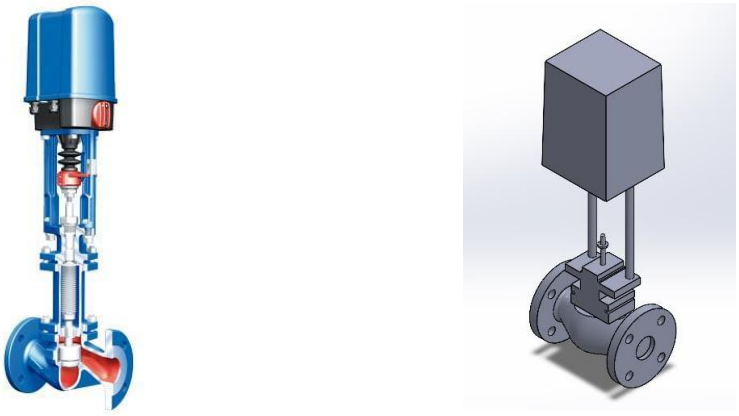

(a) (b)

**Figure 7**: (a) Ari-Stevi globe valve with Ari-Premio electric actuator, and (b) CAD model

### 3.5 Graph of Pressure Difference versus Mass Flow Rate

Figure 8 shows the result of pressure drop (differential) versus mass flow rate across the Ari-Stevi globe valve. This graph was obtained from a series of calculations at six different upstream pressure of the globe valve. Note that the highest operating pressure at the gas stand is 4 bar (absolute) as given in Table 3. Every point in the graph is plotted based on dry air at different downstream pressure and corresponding density.

At a constant mass flow rate, lower upstream pressure will result in larger pressure drops across the globe valve. This characteristic graph is useful in determining the upstream pressure of the globe valve for the desired mass flow rate. When the gas stand operates at the maximum flow rate of 0.1 kg/s, the upstream pressure can be set to as low as 2.5 bar. This would give maximum accuracy of flow control while keeping the pressure drop across the globe valve lower within 0.05 bar.

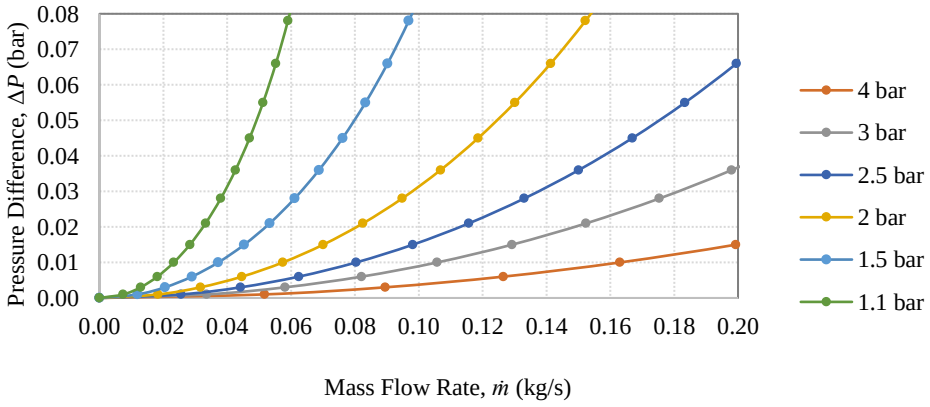


**Figure 8**: Graph of pressure difference versus mass flow

### 3.6 Final Design of the Flow Control Mechanism on Turbocharger Gas Stand

Figure 9 shows the newly designed flow control mechanism for the turbocharger gas stand. In comparison to the previous design in Figure 3, the flow piping downstream to the shut-off valve has been re-routed to make room for the new globe valve and actuator. The compressed air is first passed through the existing dryer filter to remove any moisture in the air. It then goes through the existing pressure regulator preset at the desired upstream pressure according to the characteristic graph in Figure 8. The use of this pressure regulator ensures the upstream pressure is regulated at relatively constant pressure with no major fluctuation.

 DOI: https://doi.org/10.11113/jm.v45.453

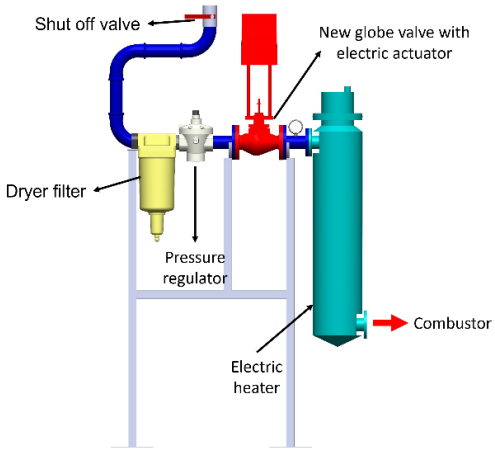


**Figure 9**: Newly designed flow control mechanism.

The airflow is then entering the new globe valve where it will be further regulated to achieve the desired testing conditions. Lastly, the regulated airflow is heated up by the existing electric heater before being fed to the turbocharger turbine. Heating the airflow ensures no condensation will happen at the turbine outlet after expansion. Though this should be done in moderation to avoid inducing additional heat transfer uncertainty. The common rule of thumb is to maintain turbine outlet temperature around ambient temperature.

The schematic diagram of the UTM LoCARtic turbocharger gas stand is shown in Figure 10, with the newly designed flow control mechanism. Figure 11 shows the isometric view of the turbocharger gas stand in CAD. For a better testing experience, the globe valve needs to be self-regulated according to the target turbocharger speed and target turbine pressure ratio. This minimizes the random error potentially caused by human control, giving rise to more precise testing data. The designed control hardware and algorithm will next be presented in detail in Section 4.5.

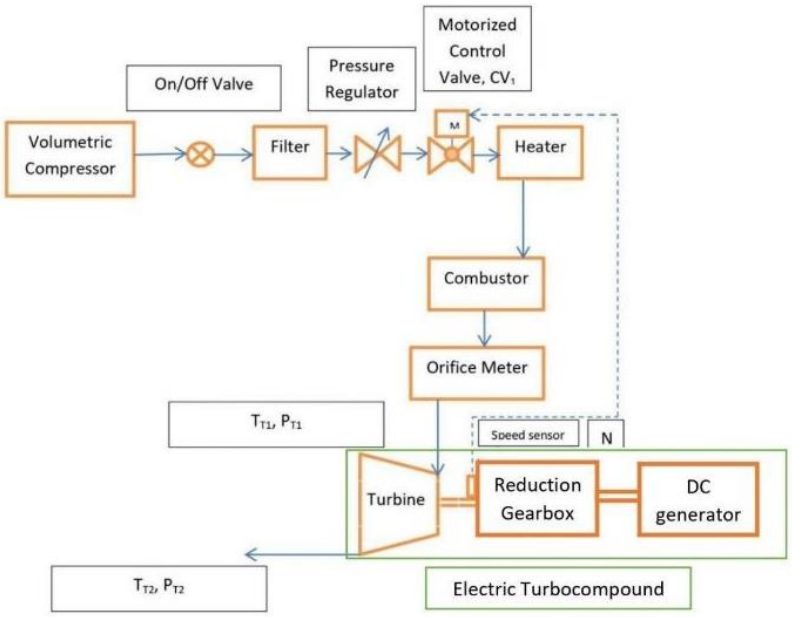


**Figure 10**: Schematic diagram of the UTM LoCARtic turbocharger gas stand with the newly designed flow control mechanism.


DOI: https://doi.org/10.11113/jm.v45.453

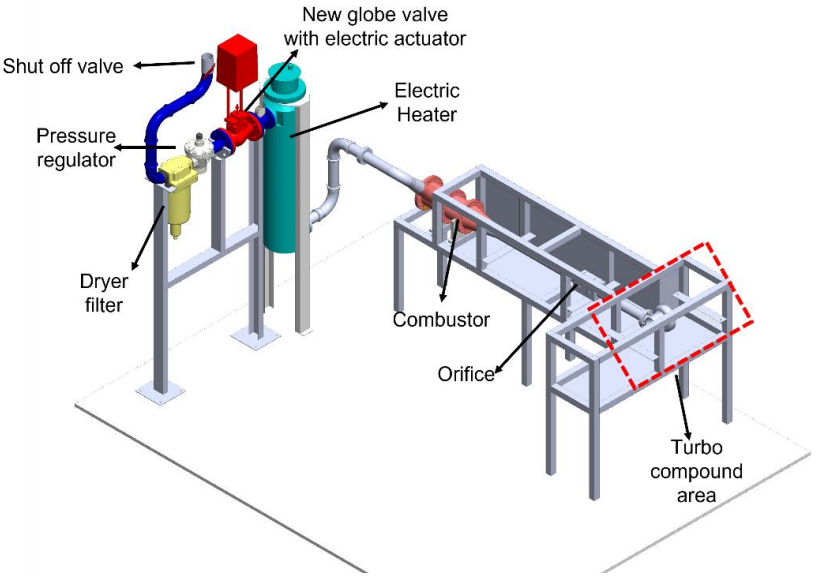


**Figure 11**: Isometric view of the UTM LoCARtic turbocharger gas stand with the newly designed flow control mechanism.

### 3.7 Control Loop Design of the New Flow Control Mechanism

A generic PID controller is adopted for the turbocharger speed control. The block diagram of the turbocharger gas stand with the ARI-PREMIO electric actuator and PID controller is shown in Figure 12. The PID controller is designed using NI LABVIEW software and deployed on the NI USB-6218 DAQ device. Figure 13 shows the PID control loop function designed using NI LABVIEW software. The PID controller updates the actuator control signal based on the current speed setpoint and sensor feedback data. The control signal range of the ES11 electronic positioner is from 0 to 10V. On the other hand, the speed range of the turbocharger is from 0 to 200kRPM.

The PID controller is tunned using trial and error method to determine the ideal gain value for the entire operating range. The tunning process start with zero proportional gain, Kp, integral gain, Ki and derivative gain,Kd. Then the Kp gain is adjusted so that the error between setpoint and measurement is about 25%. Next, the Ki gain is inserted to eliminate the steady state error and the Kd gain to improve transient response and overshoot. The process is repeated to obtain the best response time, steady state error and zero overshoot. The tuning process is carried out on the tuning subpanel, as shown in Figure 14. Figure 15 shows the front panel for the turbocharger speed control and sensors reading.

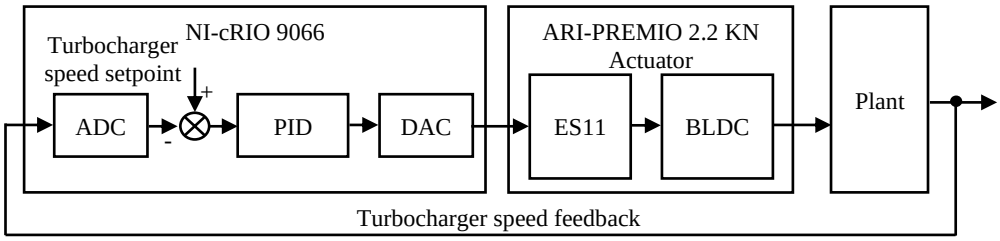


**Figure 12**: Block diagram of Turbocharger gas stand with PID Controller


DOI: https://doi.org/10.11113/jm.v45.453

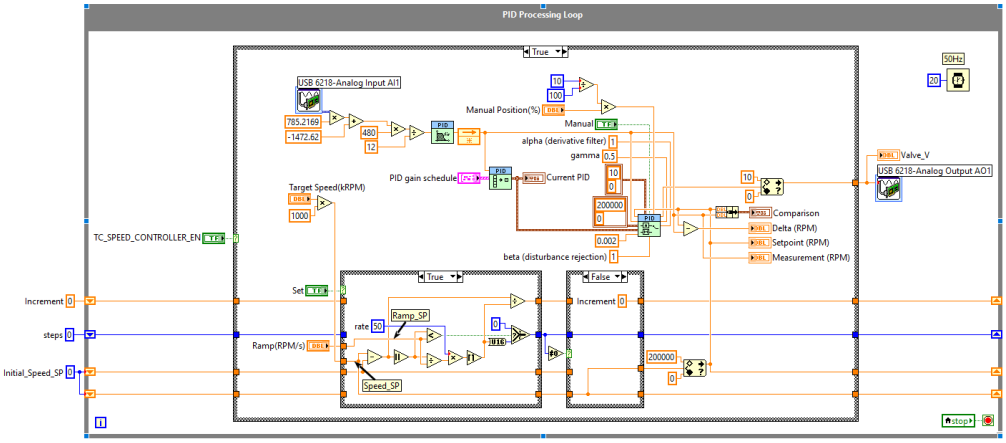


**Figure 13**: Block diagram of PID control loop

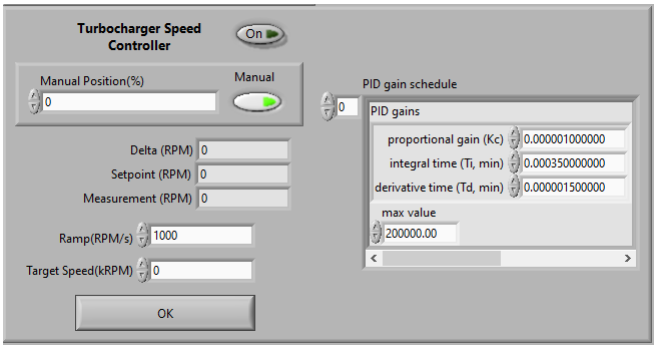


**Figure 14**: Subpanel for PID tunning

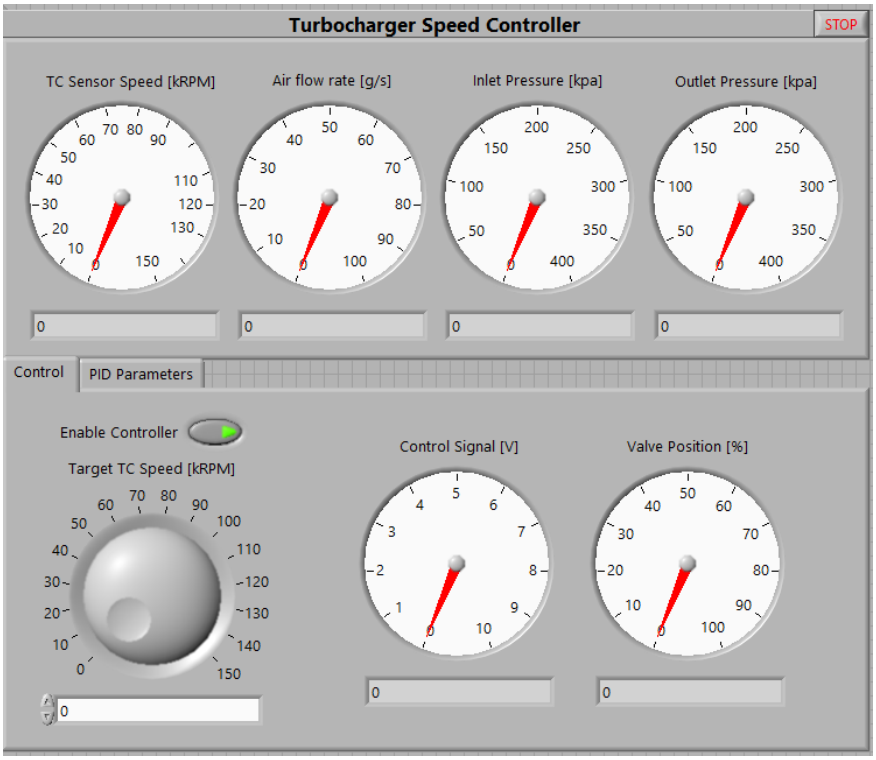


**Figure 15**: Front panel for turbocharger speed control and indicators


DOI: https://doi.org/10.11113/jm.v45.453

## 4.0 RESULTS AND DISCUSSION

This subsection will be discussed about the effect of using self-regulated valve control. Figure 16 shows the final assembly of self-regulated from control mechanism on turbocharger gas stand. Use of electric actuator glove valve allow the function of self-regulated.

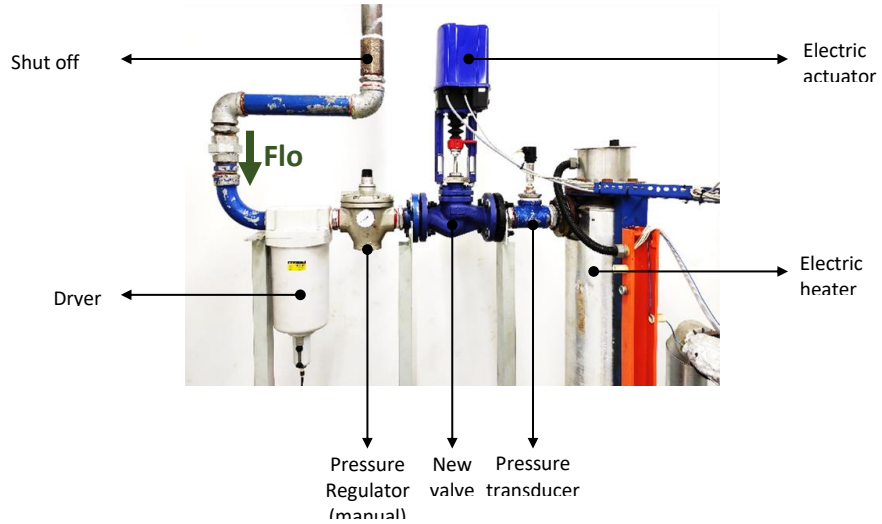


**Figure 16:** New self-regulated flow mechanism

Figure 17 shows the flow comparison at two different conditions at a constant pressure. For condition 1, the previous system can't maintain the pressure while new system with new globe valve able to main the pressure. For the previous system, target pressure is 128.0 kPa. However, due to difficulty to regulate, the target pressure deviated to 128.3 kPa and within 10 second, the pressure keeps increasing. The range of error between 0.3% to 0.6% which is consider big in turbocharger testing. With the implementation of new valve, the pressure is more stable at 129.0 kPa. Despite of some deviation, but it still I acceptable range because the deviation between 0.005% to 0.09%. In second conditions, the previous system pressure has sudden drop about 0.1%. This sudden drop is not good during turbocharger test because it disturbs the whole system and effect the heat transfer inside the turbocharger. With the implementation of new system, the pressure more stable Next, the paper will be discussed about the PID control.

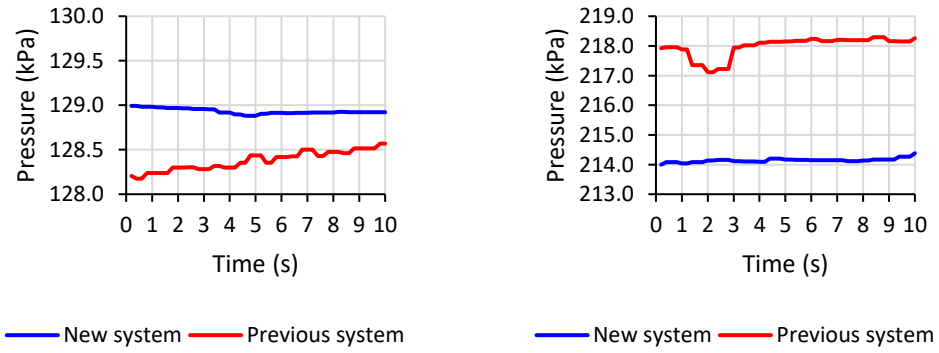


a) Condition 1 b) Condition 2

**Figure 17:** Flow comparison at two different conditions


DOI: https://doi.org/10.11113/jm.v45.453

Table 6 shows the tuned parameters for PID controller based on trial-and-error method. Next, the tuned controller is tested at 10kRPM, 30kRPM and 60kRPM operating region to observe the performance characteristic at different operating range. The turbocharger speed response at three operating range is shown in Figure 18, Figure 20 and Figure 22 respectively. The delta difference between speed setpoint and measurement at three operating range is show in Figure 19, Figure 21 and Figure 23 respectively.

**Table 6**: PID controller parameters

| Parameters | Value |
|---|---|
| Proportional gain, Kp | 0.0000010 |
| Integral gain, Ki | 0.0003500 |
| Derivative gain, Kd | 0.0000015 |

Table 7 shows the input ramp speed and chart update rate used in the experiment. A ramp speed input is used in the experiment to enable a smooth and gradual speed transition.

**Table 7**: Experiment setup condition

| Parameters | Value |
|---|---|
| Target ramp speed (RPM/s) | 2500 |
| Chart data update rate (Hz) | 2 |

Figure 18 shows the transient and steady state response from 0kRPM to 10kRPM. For this operating region, an underdamped response is seen in Figure 18 below with rise time 3 second, settling time 29 second, 24% overshoot and 3% steady state error. The 9200RPM maximum transition error and 300RPM steady state error as shown in Figure 19.

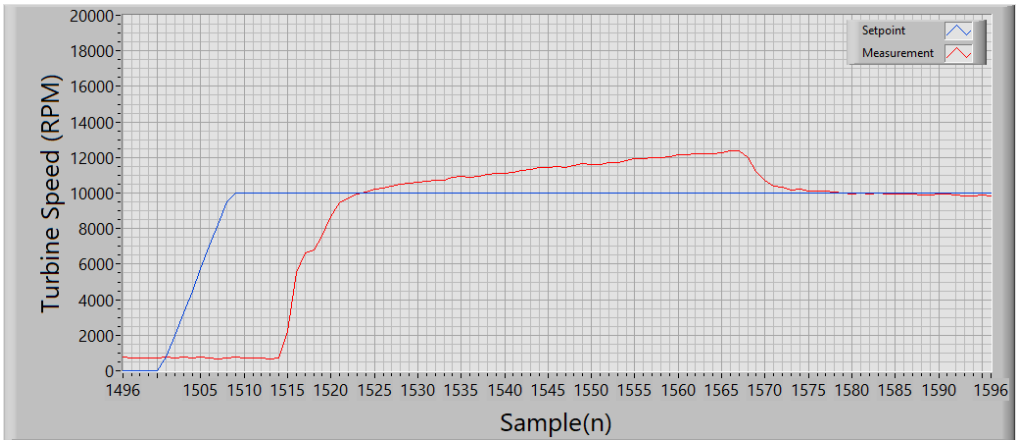


**Figure 18**: Transient and steady state response from 0kRPM to 10kRPM

 DOI: https://doi.org/10.11113/jm.v45.453

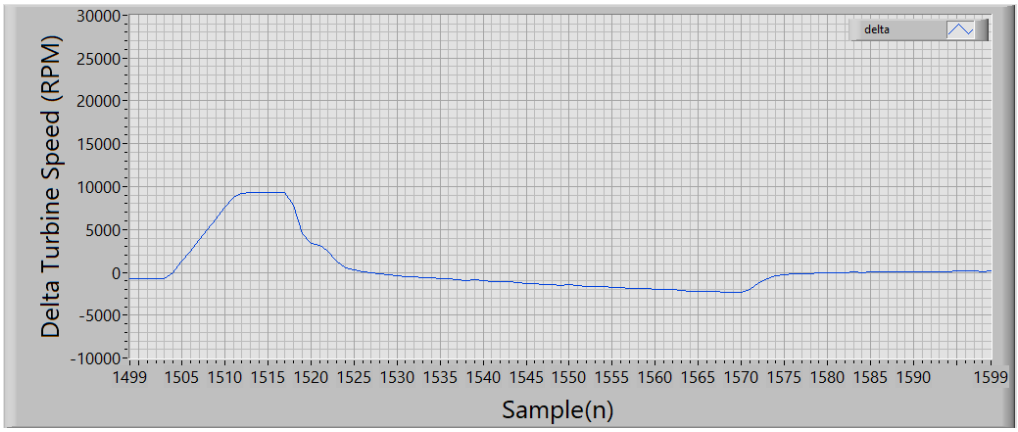


**Figure 19**: Delta error of the transient and steady state response from 0kRPM to 10kRPM

Figure 20 shows the transient and steady state response from 10kRPM to 30kRPM. For this operating region, a critically damped like response is seen in Figure 20 below with rise time 23 second, settling time 39 second, 0% overshoot and 2.66% steady state error. The 14000RPM maximum transition error and 800RPM steady state error as shown in Figure 21.

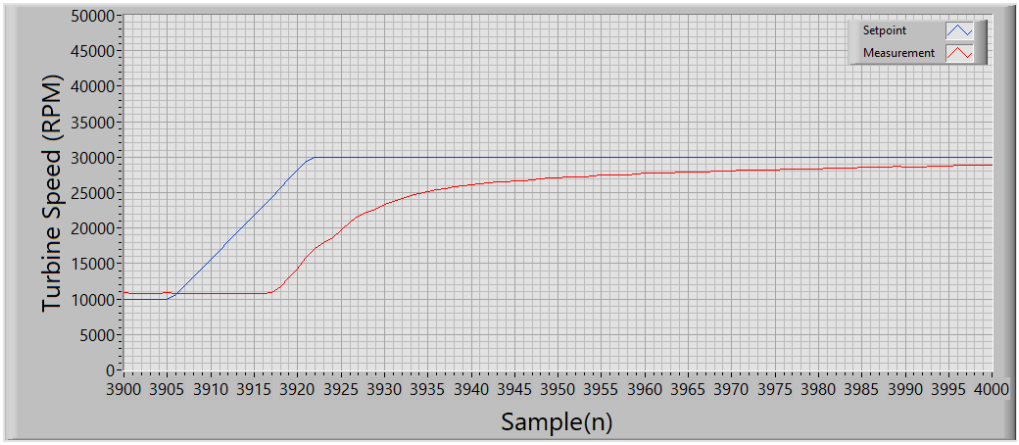


**Figure 20**: Transient and steady state response from 10kRPM to 30kRPM

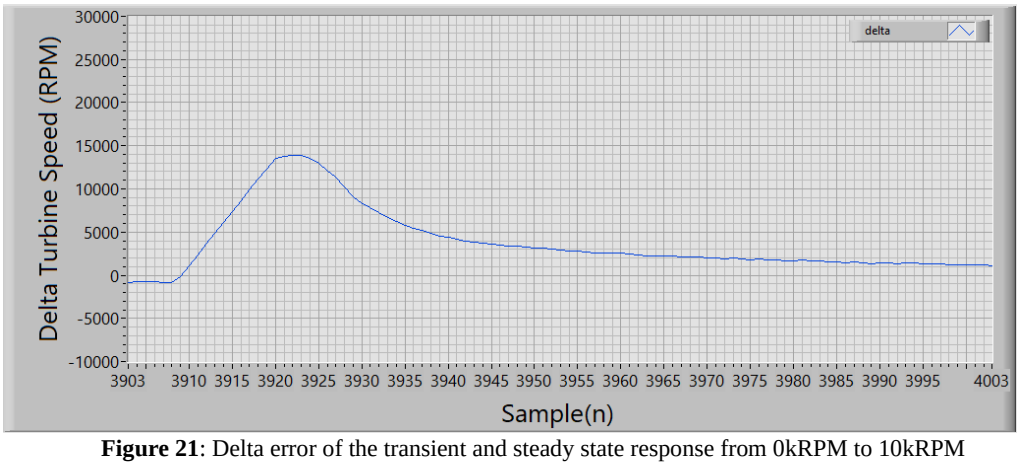


**Figure 21**: Delta error of the transient and steady state response from 0kRPM to 10kRPM

Figure 22 shows the transient and steady state response from 30kRPM to 60kRPM. For this operating region, an overdamped like response is seen in Figure 22 below with rise time 28 second, settling time 40 second, 0% overshoot and 2.5% steady

 DOI: https://doi.org/10.11113/jm.v45.453

state error. The 28000RPM maximum transition error and 1500RPM steady state error as shown in Figure 23.

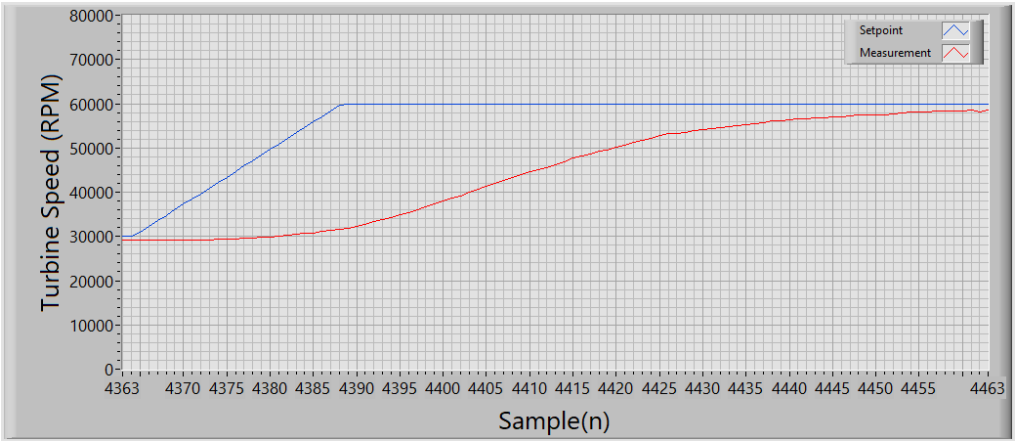


**Figure 22**: Transient and steady state response from 30kRPM to 60kRPM

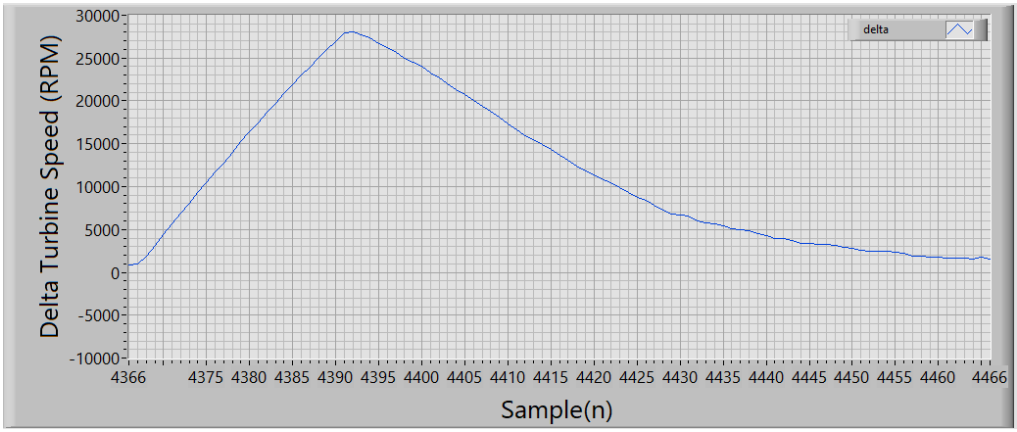


**Figure 23**: Delta error of the transient and steady state response from 30kRPM to 60kRPM

In this work, a single PID controller is used to obtain good output response for various operating region. The main PID tuning strategy is to obtain a minimum steady state error. This is because the experiment and data collection carry out on this turbocharger test stand are primary focused at a steady turbocharger speed region. Table 8 summarized the performance characteristic at three speed operating range. From this table, there is a noticeable difference in the time response between 0-10 kRPM and above 10kRPM speed operating region. Besides that, a noticeable 6 second time delay is observed between the set point and measurement data. Overall, this single PID controller setup is capable to achieve steady state error with less than 3% at various operating range. For future work, adaptive controller such as gain scheduling controller can be employed to improve the rise and settling time at high-speed operating region.

**Table 8**: Performance characteristic of turbocharger speed with PID at three speed operating range

| **Response characteristics** | **Speed operating region (kRPM)** | | |
|---|---|---|---|
| | **0 – 10** | **10 – 30** | **30 – 60** |
| Rise time (Tr) | 3s | 23s | 28s |
| Settling time (Ts) | 29s | 39s | 40s |
| Percentage overshoot (%OS) | 24% | 0% | 0% |
| Steady state error (ess%) | 3% | 3.8% | 2.1% |


DOI: https://doi.org/10.11113/jm.v45.453

## 5.0 CONCLUSION

In conclusion, this paper presented the design of a new flow control mechanism for the UTM LoCARtic turbocharger gas stand test rig. The design aims to achieve a self-regulated flow control mechanism, eliminating the operators' safety hazards at the same time obtain more precise and accurate testing results. The appropriate control valve is selected using standard valve sizing techniques based on the gas stand's requirement. The minimum flow coefficient requirement is first calculated from the maximum gas stand's operating condition. The appropriate control valves are then shortlisted for comparison, by considering their inherent flow characteristic, material and strength, flow coefficient and availability. The Ari-Steri globe valve is chosen for the current application. Its flow coefficient is sufficient for the gas stand's operation, and the electric actuator is also comparatively responsive and stronger. All these help for achieving fast, precise and accurate control during the testing. The flow control mechanism is successfully designed and assembled in CAD software. In addition, the control loop design for the new flow control mechanism is also presented.

## ACKNOWLEDGMENT

The authors would like to acknowledge the Ministry of Higher Education Malaysia (MOHE) for funding this research under the registered program cost centre: R.J130000.7809.5F111.

## NOMENCLATURE

| | | | |
|---|---|---|---|
| $K_V$ | Flow factor | $T$ | Temperature |
| $R$ | Gas constant | $P$ | Pressure |
| $\dot{m}$ | Mass flow rate | $SG$ | Specific gravity |
| $Q$ | Volume flow rate | 1 | Inlet |
| $N$ | Normal conditions | 2 | Outlet |

## REFERENCES

[1] H. Tiikoja, H. Rämmal, M. Åbom, and H. Bodén, "Test-rig for complete acoustic characterization of turbochargers," *16th AIAA/CEAS Aeroacoustics Conf. (31st AIAA Aeroacoustics Conf.*, pp. 1–9, 2010, doi: 10.2514/6.2010-4012.

[2] J. R. Serrano, F. J. Arnau, R. Novella, and M. Á. Reyes-Belmonte, "A procedure to achieve 1d predictive modeling of turbochargers under hot and pulsating flow conditions at the turbine inlet," *SAE Tech. Pap.*, vol. 1, no. February 2016, 2014, doi: 10.4271/2014-01-1080.

[3] J. Galindo, J. R. Serrano, C. Guardiola, and C. Cervelló, "Surge limit definition in a specific test bench for the characterization of automotive turbochargers," *Exp. Therm. Fluid Sci.*, vol. 30, no. 5, pp. 449–462, 2006, doi: 10.1016/j.expthermflusci.2005.06.002.

[4] X. Bian *et al.*, "A comprehensive evaluation of the effect of different control valves on the dynamic performance of a recompression supercritical CO2 Brayton cycle," *Energy*, vol. 248, p. 123630, Jun. 2022, doi: 10.1016/J.ENERGY.2022.123630.

[5] M. Agrež, J. Avsec, and D. Strušnik, "Entropy and exergy analysis of steam passing through an inlet steam turbine control valve assembly using artificial neural networks," *Int. J. Heat Mass Transf.*, vol. 156, p. 119897, Aug. 2020, doi: 10.1016/J.IJHEATMASSTRANSFER.2020.119897.

[6] J. Y. Qian, Z. X. Gao, J. K. Wang, and Z. J. Jin, "Experimental and numerical analysis of spring stiffness on flow and valve core movement in pilot control globe valve," *Int. J. Hydrogen Energy*, vol. 42, no. 27, pp. 17192–17201, Jul. 2017, doi: 10.1016/J.IJHYDENE.2017.05.190.

[7] D. Moses, G. Haider, and J. Henshaw, "An investigation of the failure of a 1/4" ball valve," in *Engineering Failure Analysis*, vol. 100, Pergamon, 2019, pp. 393–405.

[8] K. Sotoodeh, "Valve technology and selection," *A Pract. Guid. to Pip. Valves Oil Gas Ind.*, pp. 559–584, Jan. 2021, doi: 10.1016/B978-0-12-823796-0.00021-0.

[9] B. Sirakov and M. Casey, "Evaluation of Heat Transfer Effects on Turbocharger Performance," *J. Turbomach.*, vol. 135, no. 2, 2012, doi: 10.1115/1.4006608.

[10] F. Westin and R. Burenius, "Measurement of interstage losses of a twostage turbocharger system in a turbocharger test

 DOI: https://doi.org/10.11113/jm.v45.453

rig," *SAE Tech. Pap.*, 2010, doi: 10.4271/2010-01-1221.
[11] J. Andersen, F. Lindström, and F. Westin, "Surge definitions for radial compressors in automotive turbochargers," *SAE Int. J. Engines*, vol. 1, no. 1, pp. 218–231, 2009, doi: 10.4271/2008-01-0296.
[12] P. Lyttek, H. Roclawski, M. Böhle, and M. Gugau, "New modular test rig for unsteady performance assessment of automotive turbocharger turbines," *Proc. ASME Turbo Expo*, vol. 8, 2017, doi: 10.1115/GT2017-64218.
[13] J. Slota, M. Jurčišin, and E. Spišák, "Experimental and numerical analysis of local mechanical properties of drawn part," *Key Eng. Mater.*, vol. 586, no. January 2015, pp. 245–248, 2014, doi: 10.4028/www.scientific.net/KEM.586.245.
[14] "Control Valves Basics Sizing and Selection." https://www.cedengineering.com/courses/control-valve-basics-sizing-and-selection (accessed Apr. 23, 2021).
[15] S. K. Sreekala and S. Thirumalini, "Study of flow performance of a globe valve and design optimisation," *J. Eng. Sci. Technol.*, vol. 12, no. 9, pp. 2403–2409, 2017.
[16] "Control Valve Characteristics." https://instrumentationtools.com/control-valve-characteristics/ (accessed Apr. 15, 2021).
[17] "Flow Coefficient Definition," *Valvias*. http://www.valvias.com/flow-coefficient.php (accessed Apr. 01, 2021).
[18] J. Ferrari and Z. Leutwyler, "Fluid Flow Force Measurement Under Various Cavitation State on a Globe Valve Model," in *Proceedings of the ASME 2008 Pressure Vessels and Piping Conference*, Jul. 2008, pp. 157–165, doi: 10.1115/PVP2008-61238.
[19] "What's the Difference Between Pneumatic, Hydraulic, and Electrical Actuators?," *Machine Design*. https://www.machinedesign.com/mechanical-motion-systems/linear-motion/article/21832047/whats-the-difference-between-pneumatic-hydraulic-and-electrical-actuators (accessed Apr. 05, 2021).
[20] M. C. Potter, D. C. Wiggert, and B. H. Ramadan, *Mechanics of Fluids*, 5th ed. United States: Cengage Learning, 2016.
[21] Q. K. Nguyen *et al.*, "Bubble formation in globe valve and flow characteristics of partially filled pipe water flow," *Int. J. Nav. Archit. Ocean Eng.*, Jun. 2021, doi: 10.1016/j.ijnaoe.2021.06.007.
[22] Q. K. Nguyen, K. H. Jung, G. N. Lee, S. B. Suh, and P. To, "Experimental study on pressure distribution and flow coefficient of globe valve," *Processes*, vol. 8, no. 7, 2020, doi: 10.3390/pr8070875.
[23] "Proportional Solenoid Valve - How They Work." https://tameson.co.uk/proportional-solenoid-control-valve.html?cv=1https://tameson.co.uk/proportional-solenoid-control- (accessed Feb. 25, 2021).

 DOI: https://doi.org/10.11113/jm.v45.453